Journal of Power Sources 270 (2014) 318–325

Contents lists available at ScienceDirect

Journal of Power Sources

journal homepage: www.elsevier.com/locate/jpowsour

High performance lithium-ion hybrid capacitors with pre-lithiated hard carbon anodes and bifunctional cathode electrodes

Xianzhong Sun, Xiong Zhang, Haitao Zhang, Nansheng Xu, Kai Wang, Yanwei Ma*

Key Laboratory of Applied Superconductivity, Institute of Electrical Engineering, Chinese Academy of Sciences, Beijing 100190, PR China

HIGHLIGHTS

- Hard carbon, graphite and mesocarbon microbeads were investigated for Lithium-ion hybrid capacitors.
- A facile approach to achieve the pre-lithiation of carbonaceous anode was developed.
- Electrode potentials of hybrid capacitors were monitored during the galvanostatic charge–discharge processes.
- Hybrid capacitor shows high energy density, high power density and superior cycleability.

GRAPHICAL ABSTRACT

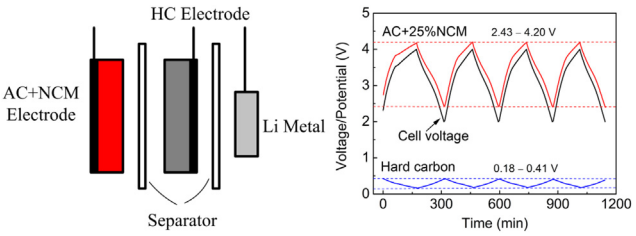

ARTICLE INFO

Article history:
Received 17 April 2014
Received in revised form
26 June 2014
Accepted 22 July 2014
Available online 30 July 2014

Keywords:
Lithium ion hybrid capacitor
Pre-lithiation
Hard carbon
Activated carbon

ABSTRACT

Lithium-ion hybrid capacitor is a type of energy storage device that bridge the gap between lithium-ion battery and electrical double layer capacitor. We have developed a facile approach to achieve the pre-lithiation of carbonaceous anode, and then fabricated lithium-ion hybrid capacitors with bifunctional cathode containing capacitor material (activated carbon) and battery material ($LiNi_{0.5}Co_{0.2}Mn_{0.3}O_2$). The hybrid capacitor with 25 wt.% $LiNi_{0.5}Co_{0.2}Mn_{0.3}O_2$ addition in bifunctional cathode (denoted as LAN25) exhibits excellent rate capability and high energy density. The rate capability of LAN25 is comparable to that with pure AC cathode (denoted as LAC), while the volumetric energy density is 1.36 times higher than the latter one. The continuous galvanostatic charge–discharge cycling tests reveal that the lithium-ion hybrid capacitor remains more than 98% capacity after 20,000 cycles, and nearly 100% coulombic efficiency over entire cycles. The superior performance is ascribed to the synergy effect of the active components in bifunctional cathode and the effective pre-lithiation of hard carbon anode. The present work makes the study of lithium-ion hybrid capacitor easily accessible and broadens roads to hybrid devices with high energy density, high power density and long cycle life.

1. Introduction

Lithium-ion battery (LIB) and electrochemical capacitor (EC) are two important types of electrochemical energy storage devices that can be used in hybrid renewable energy power generation/energy storage systems, electric vehicles (EVs) and hybrid electric vehicles (HEVs) [1]. LIB displays relatively high energy density but limited power density and cycle life. EC possesses high power capability and superior cycleability, however, the specific energy is much lower than that of LIB [2,3]. The internal hybrid systems can be designed to combine the advantages of both LIB and EC by the synergetic hybridization of the battery and capacitor components [4].

* Corresponding author. Tel.: +86 10 82547129; fax: +86 10 82547137.
E-mail address: ywma@mail.iee.ac.cn (Y. Ma).

http://dx.doi.org/10.1016/j.jpowsour.2014.07.146
0378-7753/

The internal serial/parallel hybridization approaches can be achieved employing the lithium-ion intercalation materials and the electrical double layer capacitive materials within one device [5]. Generally, these kinds of hybridizations are called lithium-ion capacitors or lithium-ion hybrid capacitors (LICs). Amatucci and Du Pasquier et al. [6,7] firstly reported the internal serial hybridization system using activated carbon (AC) as capacitive component (cathode), and $Li_4Ti_5O_{12}$, graphite, or WO_2 as battery component (anode). After that, carbonaceous materials for LICs, e.g., graphite [8–10], soft carbon [11,12], hard carbon [13], graphene nanosheets [14], carbon nanofiber [15], amorphous carbon [16], and the internal serial hybridization systems [17–22] were extensively investigated and even successfully commercialized by some Japanese companies including JM Energy, FDK, ACT, etc. On the other side, the internal parallel hybridization system within one device can be prepared by using at least one bifunctional electrode including both capacitive material and lithium-ion intercalation material, e.g., ($LiCoO_2$-AC)/$Li_4Ti_5O_{12}$ [3], ($LiFePO_4$-AC)/$Li_4Ti_5O_{12}$ [23–25], ($LiMn_2O_4$-AC)/$Li_4Ti_5O_{12}$ [26], and ($LiMn_2O_4$-AC)/($Li_4Ti_5O_{12}$-AC) [5,27,28].

In our previous work [29], the internal hybrid energy storage devices have been prepared by employing (AC + $LiNi_{0.5}Co_{0.2}Mn_{0.3}O_2$ (NCM)) bifunctional electrode as cathode and graphite electrode as anode. The hybrid device with a (25 wt.% AC+75 wt.% NCM) cathode possesses a specific energy 5.7 times higher than that of electrical double layer capacitor (EDLC) with nonaqueous electrolyte of tetraethyl ammonium tetrafluoroborate (Et_4NBF_4) in acetonitrile (AN). At the same time, the hybrid device delivers 62.6% and 42.1% of its maximum capacity at the rate of 30C and 50C, respectively. Besides, it shows stable capacity retention and high coulombic efficiency over 2000 electrochemical cycles. However, it is found that the experimental specific capacities of the composite cathodes are much smaller than the theoretical capacities. From the CV curves of the (AC + NCM)/graphite hybrid devices, no obvious peaks corresponding to the sequential phase transition processes ($Ni^{2+} \leftrightarrow Ni^{3+} \leftrightarrow Ni^{4+}$) appear when the relative amount of NCM in the total active materials is not larger than 0.5, i.e., $r = m_{NCM}/(m_{AC} + m_{NCM}) \leq 0.5$. It implies that most of Li ions deintercalated from NCM in the initial charge process did not insert back. These Li ions were consumed when the solid electrolyte interphase (SEI) films formed on graphite electrode surface [30,31]. The competing relationship exists between the ionic adsorption of electrical double layer contributed by AC and the faradaic electrochemical process (redox reaction) caused by Li ion intercalation in composite cathode. In general, the surface adsorption/desorption process is much faster than the Li ion intercalation/de-intercalation reaction, thus the faradaic process is suppressed. In the subsequent charge–discharge cycles, the cathode cannot be fully discharged, leading to the low capacity and low energy density. Therefore, it is necessary to pre-dope Li ions into carbonaceous anode to reduce the irreversible capacity loss.

Generally, the pre-lithiation of carbon anode is carried out using the following methods [16,32]: (1) the lithium foil and the carbon electrode are separated by a separator in a Li-to-carbon arrangement, and then the cell is externally shorted or electrochemically discharged; (2) the carbon electrode directly contacts with the lithium foil in electrolyte without electronic charger or external electric circuit; (3) the special aluminum/copper foils with through holes are employed as current collectors of cathode and anode, a lithium foil is used as a lithium source. This configuration allows Li ions to transport through the holes of current collector. For the former two methods, the cells would be disassembled after the lithiation process completed, and the full cell with cathode and lithiated anode is rearranged in an operating configuration. By the latter method, the rearrangement step can be eliminated. Furthermore, in this work, we found that the carbon electrode could be well lithiated by using ordinary Al/Cu foils instead of expensive through-hole Al/Cu foils.

To date, graphite is the most widely used anode material in commercial LIBs and LICs due to its low negative redox potential (~0.1 V vs. Li^+/Li), high theoretical capacity (372 mAh g^{-1} for LiC_6 stoichiometry) and relatively low cost. However, the power capabilities of devices are restricted by the poor charge rate (Li ion intercalation) capability of graphite electrode due to the limitations of Li ion diffusion into the bulk structure [10]. In addition, the potential plateau of graphite anode electrode is so close to the potential of metal lithium plating, which increases the risk of lithium dendrites formation and growth on the surface of anode at high charge current, causing the internal short-circuits failure of a cell.

In the present work, we proposed a novel LIC structure using a hard carbon anode and a bifunctional cathode (AC + NCM). The hybrid capacitor can be regarded as an internal parallel combination of one LIC (AC/hard carbon) and one LIB (NCM/hard carbon). In order to pre-dope lithium ions into the anode electrode and monitor the potential changes of cathode and anode electrodes, a three-electrode cell with flexible package was introduced, in which a metal lithium foil was used as both a lithium source and a reference electrode. On this basis, the electrochemical performances of the hybrid capacitors were studied.

2. Experimental

$LiNi_{0.5}Co_{0.2}Mn_{0.3}O_2$ powders (NCM) were provided by Hebei Strong-Power Li-ion Battery Technology Corporation, China. AC powders (YP50F) was purchased from Kuraray Chemicals, Japan. Hard carbon (HC) was purchased from ATEC, Japan. The electrolyte is 1 M lithium hexafluorophate ($LiPF_6$) in the mixture solvent of ethylene carbonate (EC), dimethyl carbonate (DMC), and diethyl carbonate (DEC) in a volume ratio of 1:1:1, provided by Beijing Institute of Chemical Research, China. The separator is 25-μm-thick Celgard 2400 (Celgard company, USA). All the chemicals were used as received without any further treatment.

All the electrodes were prepared by a doctor-blade casting process. The composite electrodes consist of 80 wt.% active materials (AC and NCM), 10 wt.% Super C45, 2 wt.% KS-6, and 8 wt.% poly(vinylidene fluoride) (PVdF). The graphite electrode contains 90 wt.% HC, 5 wt.% Super C45, 2 wt.% styrene-butadiene rubber (CMC), and 3 wt.% styrene-butadiene rubber (SBR). The current collectors for cathode and anode electrodes are 20-μm-thick aluminum foil and 12-μm-thick copper foil, respectively. The electrodes were dried thoroughly and punched into suitable sizes: 13-mm-diameter circular discs for CR2032 coin cells, and 35 mm × 40 mm squares for three-electrode full cells.

The schematic structure of a three-electrode pouch cell is depicted in Fig. 1. The cell was prepared according to the following steps: firstly, cathode electrode, separator and anode electrode were stacked together with a sandwich structure (cathode–separator–anode), which was then inserted into an aluminum-plastic bag by following an overnight drying process under heating and vacuum. After excess electrolyte was added in a glove box (MBRAUN, H_2O < 0.1 ppm, O_2 < 0.1 ppm), a lithium foil was placed near the anode, separated by a separator. Finally, the flexible aluminum-plastic package was heat-sealed. The lithium pre-doping was accomplished by electrochemical discharge process (lithium intercalation) of HC anode using the lithium metal foil as counter electrode. The current density for pre-lithiation is 6 mA g^{-1}, and the discharge specific capacity is about 120 mAh g^{-1} (based on HC mass). The typical voltage profile of pre-lithiation process for HC anode is depicted in Fig. 2.

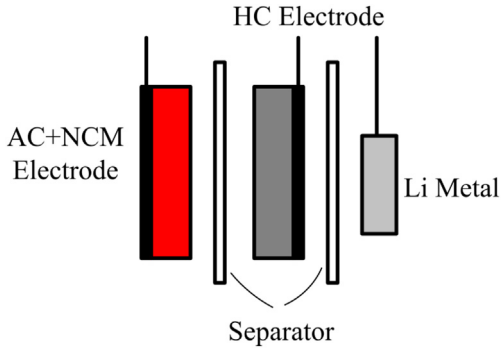

Fig. 1. Schematic structure of three-electrode lithium-ion hybrid capacitor.

The galvanostatic charge–discharge measurements were conducted using LAND CT2001A battery testers and an Arbin MSTAT 4 system. Unless otherwise specified, the values of current density and specific capacity were calculated based on the mass of active materials in cathode. The energy density and power density were calculated from the constant current discharge curves. The energy density was obtained according to the formula [33]:

$$E = \int UdC = I\int Udt/m \tag{1}$$

and the average power density was calculated using the formula:

$$P = U_m I/m \tag{2}$$

Here, C is the cell specific capacity, U is the cell voltage, U_m is the average discharge voltage, I is the current, and m is the weight of total active materials in both cathode and anode.

3. Results and discussion

The electrochemical performances of three types of carbonaceous materials for anode were comparatively studied. They are artificial graphite (CAG, Shanshan Tech., China), graphitized mesocarbon microbeads (MCMB, BTR New Energy Material Co., China), and hard carbon (HC, ATEC Co., Japan). The physical parameters including average particle diameters, Brunauer–Emmett–Teller (BET) specific surface areas and tap densities provided by suppliers are summarized in Table 1. Fig. 3a shows the voltage profile curves of carbonaceous electrode/Li coin cells measured at the current density of 100 mA g^{-1}. The specific capacities of CAG, MCMB and HC are 275.8, 350.7 and 208.1 mAh g^{-1}, respectively. For the CAG and MCMB electrodes, the curves show sloping profiles from ~1.1 to 0.19 V during the discharge process (lithium intercalation), and relatively flat plateaus below 0.19 V due to the stepwise lithium intercalation into graphene layers. On the contrary, voltage profile of the HC electrode slops down during the lithium intercalation process without showing any noticeable plateau, which is ascribed to the disordered crystal structure of HC [13]. Fig. 3b shows the differential capacity *versus* voltage (dQ/dV) curves of the carbonaceous materials. For CAG electrode, three stages of lithium ion intercalation/de-intercalation are observed, occurring below ~0.3 V with distinct redox peaks at 0.17/0.26, 0.09/0.17 and 0.05/0.14 V. The MCMB electrode exhibits similar discharge-charge characteristic. However, the anodic/cathodic curves for HC electrode show linear-like shapes except for two couples of broad peaks at 0.04/0.12 and 1.25/1.26 V. Fig. 3c reveals the reversible specific capacities at the current densities of 100, 200, 500, 1000 and 2000 mA g^{-1}. The specific capacity of CAG electrode decreases greatly as the increase of current density, and only remaining 10.0 mAh g^{-1} at 2000 mA g^{-1}. The MCMB electrode possesses moderate rate capability, and the HC electrode has the superior rate performance. The reversible specific capacity of HC at 2000 mA g^{-1} is still 92.9 mAh g^{-1}. From the structural viewpoint, hard carbon is highly irregular and disordered, primarily composed of closely and randomly connected single-layer graphene, which can be described as a “falling card” model [34]. As the space gap between the adjacent carbon layers is larger than graphite, HC material delivers a superior power capability due to the enhancement of Li ion mobility during the charge/discharge process.

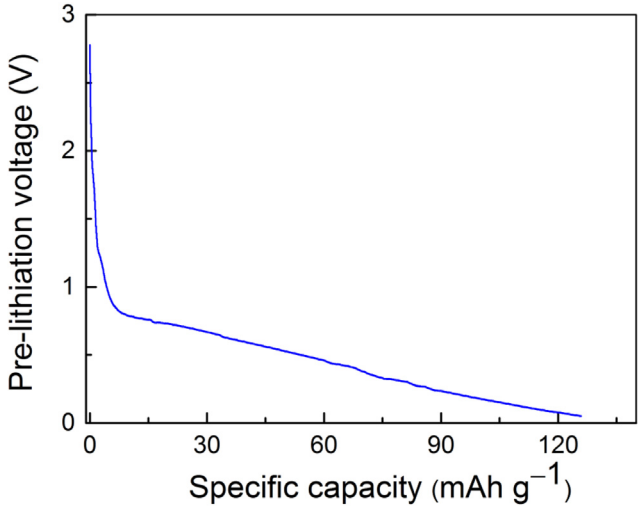

Fig. 2. Typical voltage profile of pre-lithiation process for HC anode.

Fig. 4a shows the voltage profile of (NCM + AC)/Li coin cells in the voltage range of 2.5–4.1 V at a current density of 25 mA g^{-1}. The pure NCM cathode possesses the highest specific capacity of 132.5 mAh g^{-1}, and the specific capacity of bifunctional cathode decreases with the content of NCM. As we know from our previous research [29], the specific capacity of AC electrode is 38.6 mAh g^{-1}, and the specific capacity of composite electrodes can be estimated according to Equation (3) as suggested by Fernando [35] and Böckenfeld [25], and list in Table 2.

$$C_{cal} = C_{cal-NCM} + C_{cal-AC} = 132.5r + 38.6(1-r) \tag{3}$$

Here, r is the relative amount of NCM; C_{cal} is the calculated specific capacity of composite electrode; $C_{cal\text{-}AC}$ and $C_{cal\text{-}NCM}$ are the capacity contributions of AC and NCM, respectively. For $r = 0.25$, 0.50 and 0.75, the values of C_{cal} are, respectively, 60.28, 85.55 and 109.03 mAh g^{-1}, and the corresponding ratio of capacitive contributions to the total capacities ($C_{cal\text{-}AC}/C_{cal}$) are 0.47, 0.23 and 0.09. The calculated specific capacities are much higher than the values of the hybrid cells without lithium pre-doping processes reported in our previous publication [29], which are only 25.1, 52.3 and 83.1 mAh g^{-1}, respectively. The reduced capacities are ascribed to the lithium ion assumptions on the graphite surface during the SEI

Table 1
Physical parameters of three types of carbonaceous materials: average particle diameter, BET specific surface area and tap density.

Material	Average diameter (μm)	BET surface area ($g\ m^{-2}$)	Tap density ($g\ ml^{-1}$)
CAG	11.3	1.4	1.20
MCMB	11.5	1.3–2.1	1.10–1.35
HC	5–15	8	0.77

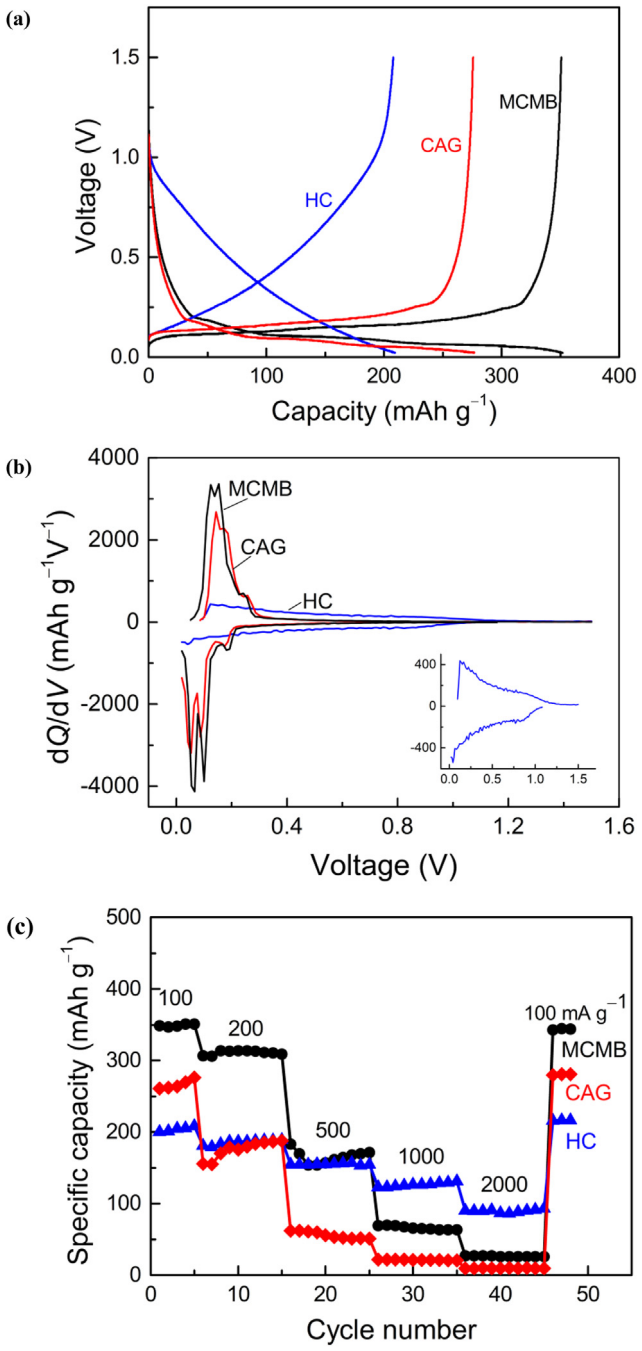

Fig. 3. Electrochemical characteristics of carbonaceous electrode/Li coin cells: (a) voltage profiles at a current density of 100 mA g^{-1}, (b) differential capacity *versus* voltage curves, insets are the magnified curves for HC electrode, (c) rate capabilities at the current densities from 100 to 2000 mA g^{-1}.

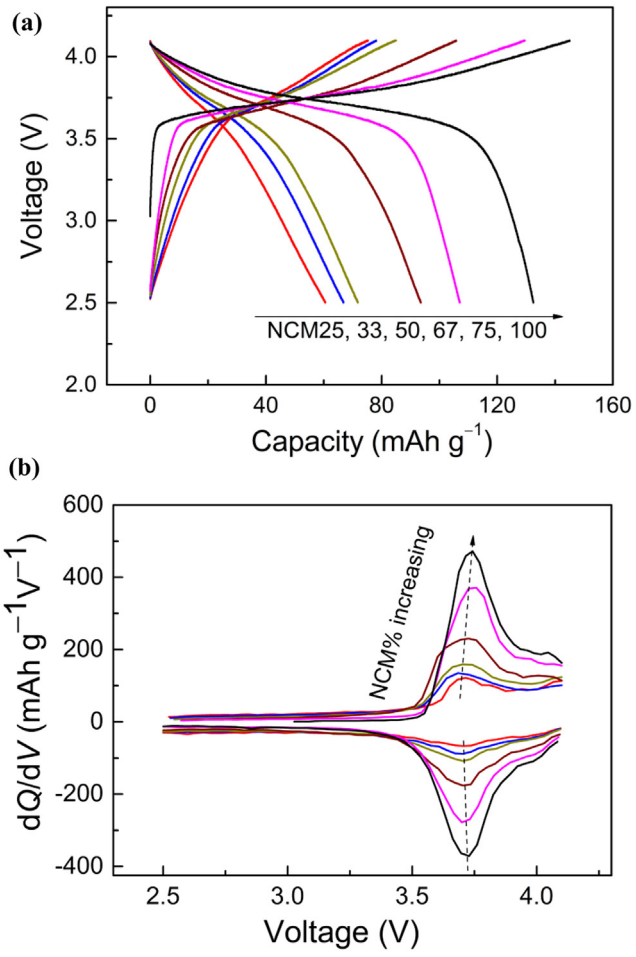

Fig. 4. (a) Voltage profiles and (b) *dQ*/*dV* curves of (AC + NCM)/Li coin cells.

film formation. Furthermore, the measured specific capacities for (NCM + AC)/Li coin cells are nearly equal to the calculated values, confirming the internal parallel hybridization behavior of capacitor material and battery material [28,36]. Fig. 4b presents the *dQ*/*dV* curves of coin cells. The redox peaks of NCM can be found in all the curves, and the intensities increase with the NCM percentage in composite electrodes.

In order to monitor the potentials of both anode and cathode electrodes of hybrid capacitors during the electrochemical cycles, the three-electrode full cells using pre-lithiated HC anode and bifunctional cathode electrode were assembled, and the details of each electrode including weight, thickness, areal density and bulk density are list in Table 3. The hybrid capacitors using AC, NCM25, NCM50 and NCM75 cathode are denoted as LAC, LAN25, LAN50, LAN75, and the weight ratio of active materials in cathode to that in anode (m_+/m_-) is 0.69, 0.79, 1.0 and 1.0, respectively. The three-electrode cells were galvanostatically charged and discharged in the voltage range between 2.0 and 4.0 V at a constant current density of about 25 mA g^{-1}. The voltage and the potential profiles vs. Li^+/Li reference electrode for both cathode and anode electrodes are shown in Fig. 5a–d. The voltage/potential *versus* time curves for LAC are linearly proportional to the charge/discharge time within the cell voltage window. The cathode and anode potentials swing from 2.39 to 4.20 V and from 0.16 to 0.38 V vs. Li^+/Li, respectively. For LAN25, the cell voltage and the cathode potential profiles reveal

Table 2
Calculated and experimental specific capacities for (AC + NCM) composite electrodes.

Electrode	*r* value	Calculated specific capacity (mAh g^{-1})				Experimental specific capacity C_{exp} (mAh g^{-1})
		C_{cal}	$C_{cal\text{-}AC}$	$C_{cal\text{-}NCM}$	$C_{cal\text{-}AC}/C_{cal}$	
NCM25	0.25	62.08	28.95	33.13	0.47	60.5
NCM33	0.33	69.59	25.86	43.73	0.37	66.8
NCM50	0.50	85.55	19.30	66.25	0.23	71.8
NCM67	0.67	101.51	12.74	88.78	0.13	93.6
NCM75	0.75	109.03	9.65	99.38	0.09	107.0

Table 3
Summary of electrode parameters for lithium-ion hybrid capacitors.

Cell	Electrode	*r* value	Electrode weight[a] (mg)	Thickness (μm)	Area (cm^2)	Areal density[b] ($g\ m^{-2}$)	Bulk density[b] ($g\ cm^{-3}$)
LAC	AC	0	49.70	58	14.0	35.50	0.61
LAN25	NCM25	0.25	56.70	51	14.0	40.50	0.79
LAN50	NCM50	0.50	72.11	52	14.0	51.51	0.99
LAN75	NCM75	0.75	71.60	35	14.0	51.14	1.46
–	HC	–	65.80	50	14.0	47.00	0.94

[a] Including the weight of active materials, conductive additives and binders.
[b] Based on the electrode weight.

obvious battery characteristic due to the capacity contribution of NCM (53% in theory). Because the capacity ratios of cathode to anode are high for LAN50 and LAN75, the potential ranges decrease to 2.46–4.10 V and 2.53–4.04 V, respectively. Fig. 5e indicates the *dQ*/*dV* curves of the hybrid capacitors during the charge–discharge processes. Comparing to the *dQ*/*dV* curves for the coin cells, the curves of full cells with bifunctional cathode show wider redox peaks due to the influences of potential change in anode electrodes.

The specific capacity as a function of current density is shown in Fig. 5f. The specific capacity based on the mass of active materials in cathode is 39.3, 55.0, 80.9 and 111.4 mAh g^{-1} for the four cells, respectively, which are very close to the aforementioned theoretical values. This indicates that the HC anodes were effectively pre-lithiated in the initial lithiation process and few lithium ions were consumed during the following charge–discharge processes. It is observed that the specific capacity of LAN25 cell is 1.38 times

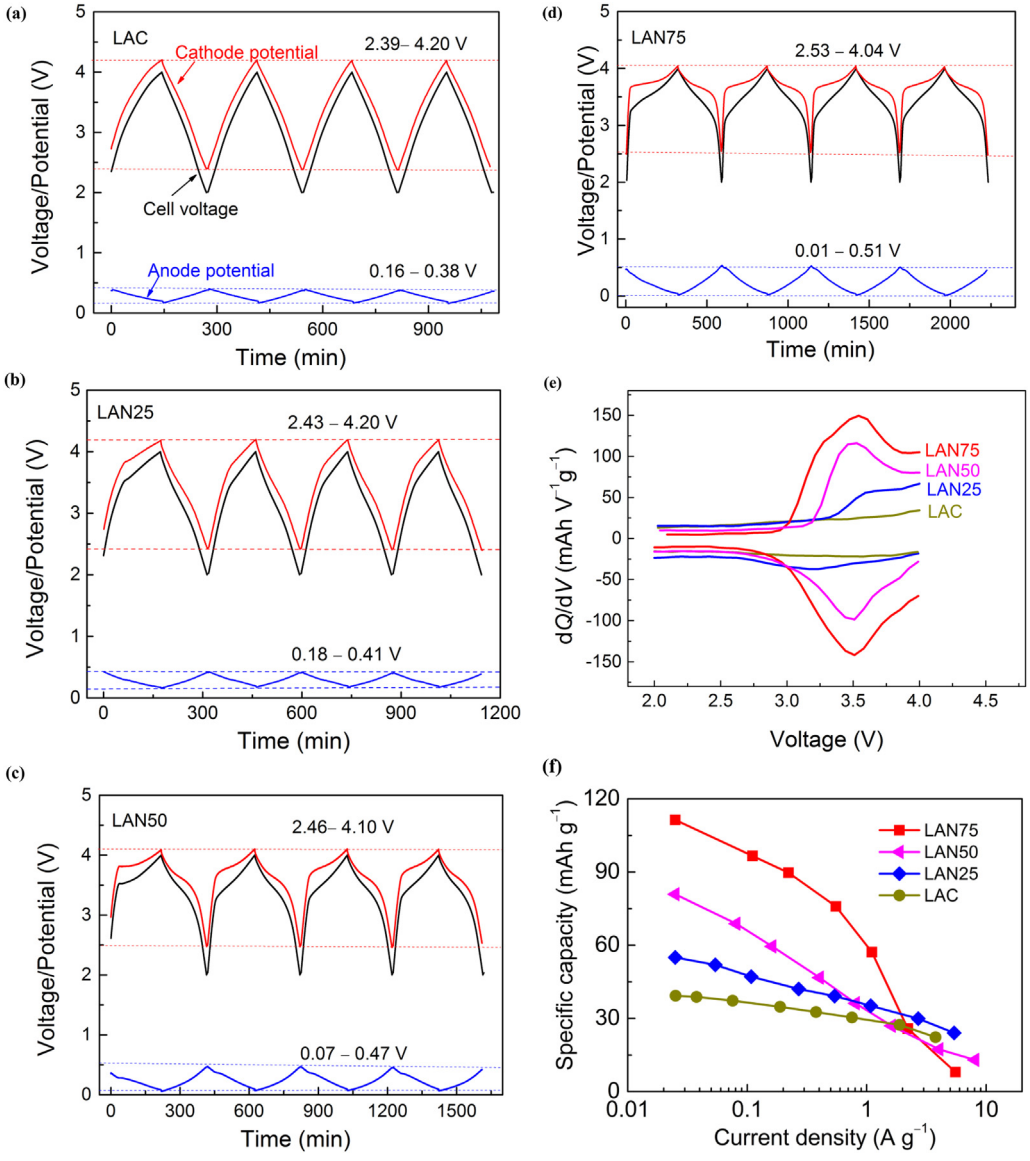

Fig. 5. Galvanostatic charge–discharge profiles during the first four cycles for three-electrode full cells in the voltage range of 2.0–4.0 V: (a) LAC, (b) LAN25, (c) LAN50 and (d) LAN75; (e) *dQ*/*dV* curves of (AC + NCM)/pre-doped HC cells; (f) specific capacity as a function of current density for the (AC + NCM)/pre-doped HC cells.

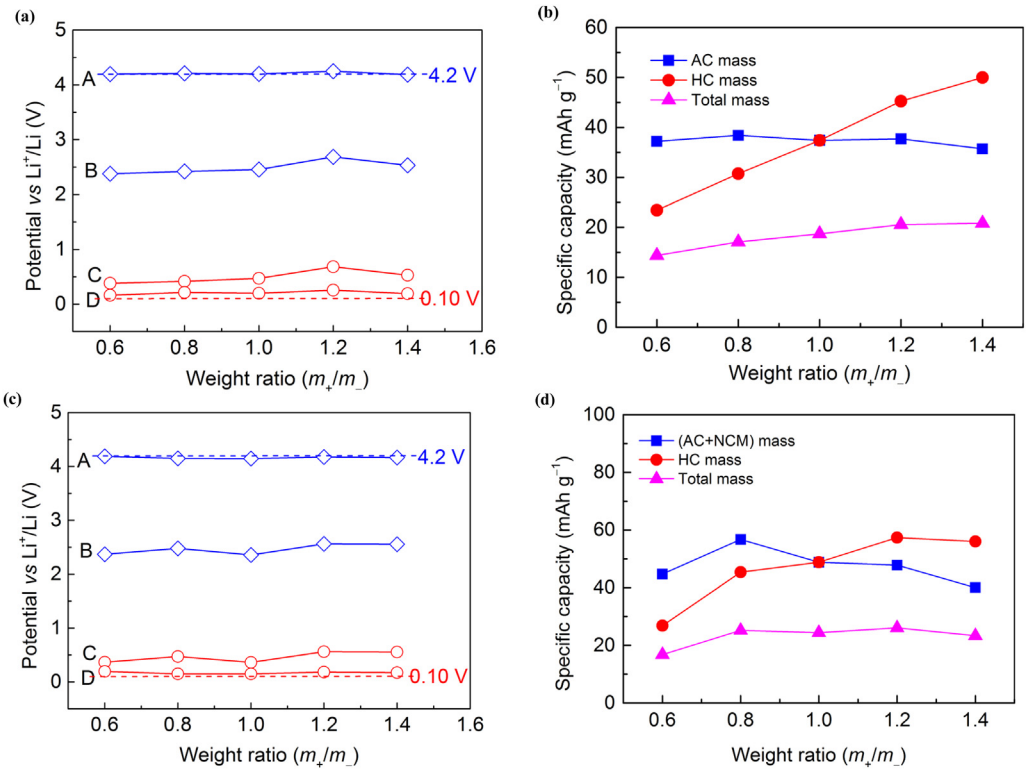

Fig. 6. Potential *versus* weight ratio curves for (a) LAC and (c) LAN25: (A) the maximum and (B) the minimum potentials of cathode, and (C) the maximum and (D) the minimum potentials of anode; and specific capacity *versus* weight ratio curves for (b) LAC and (d) LAN25.

higher than that of LAC cell. Meanwhile, its rate capability is comparable to that of the later. As the battery contributions dominate the charge storage in cathode electrode, the specific capacities for LAN50 and LAN75 decrease greatly with the increase of current density.

Furthermore, we investigated the influence of the weight ratio of active materials in cathode to that in anode (m_+/m_-) on the electrode potentials and the specific capacities of LAC and LAN25, as shown in Fig. 6a–d. As the hybrid capacitors are charged and discharged in the range of 2.0–4.0 V, the maximum potentials of cathode remain less than 4.2 V vs. Li^+/Li and the minimum potentials of anode higher than 0.1 V vs. Li^+/Li, which does not changed significantly with the weight ratios. The specific capacities based on the mass of HC increase with the increase of the weight ratios. On the other hand, the specific capacities for AC and (AC + NCM) slightly decrease due to the narrowing of the potential range of cathode. On the whole, an increase with the weight ratio can be observed for the overall specific capacity based on total activated materials in both cathode and anode. The optimal weight ratio for LAC and LAN25 is thought to be 1.2.

The energy density and the power density for LAC and LAN25 cells with optimal weight ratio are calculated on the basis of both cathode and anode electrode and displayed by Ragone plots in Fig. 7a (gravimetric) and Fig. 7b (volumetric, on the base of the electrode volume). The gravimetric energy densities are 63.6 Wh kg^{-1} at 44.8 W kg^{-1} and 75.6 Wh kg^{-1} at 41.7 W kg^{-1} for LAC and LAN25 cells, respectively. The energy densities for the LAC and LAN25 cells remain 30.9 Wh kg^{-1} at about 6.1 kW kg^{-1} and 28.5 Wh kg^{-1} at 6.9 kW kg^{-1}, respectively. As the bulk density of composite electrode is much higher than AC electrode, the LAN25 cell demonstrates a much higher volumetric energy density than LAC cell. For example, the volumetric energy density is 39.5 Wh L^{-1} at 27.8 W L^{-1} for the LAC cell, and 57.3 Wh L^{-1} at 29.6 W L^{-1} for the LAN25 cell. In contrast, the maximum gravimetric and volumetric energy densities of LAN25 cell are 3 and 5 times higher than that of EDLC with Et_4NBF_4/AN electrolyte, respectively [37]. Fig. 8 shows the continuous galvanostatic charge–discharge cycling performance of the LAC ($m_+/m_- = 0.69$) and LAN25 ($m_+/m_- = 0.75$) cells during the voltage range of 2.5–3.9 V at a current density of 0.5 A g^{-1}. The hybrid Li-ion capacitors reveal superior cycleability, with capacity retentions of more than 98% after 2×10^4 cycles for LAC and LAN25 cells, and nearly 100% coulombic efficiency over entire cycles.

Considering that the specific capacity and tap density of AC in cathode are much smaller than that of carbonaceous active materials in anode, if we want to improve the energy density of the internal serial hybridized capacitor (e.g., LAC), the thick AC cathode electrode is necessary to achieve an ideal cathode/anode capacity ratio. However, the increase of electrode thickness would lower the rate performances due to the increased internal resistance and electrochemical polarization [38]. Besides, the volumetric energy density of hybrid capacitor is limited by the low density of AC electrode. From these points of view, it is especially essential to employ bifunctional cathode electrode to obtain high energy density device. During the charge process of hybrid capacitor with bifunctional cathode, lithium ions were extracted from NCM particles and PF_6^- ions were adsorbed on AC surfaces to form electrical double layer simultaneously. During the discharge process, lithium ions were inserted back whilst the double layer were depleted. Furthermore, the battery material (NCM) and the capacitor material (AC) can display synergy in terms of material structure and energy storage [36]. As mentioned above, the specific capacity and energy density of cathode can be improved remarkably by the addition of battery materials, but the rate capability would be deteriorated due to the reduce of the capacitor component. Thus, it is an issue to balance the mass ratio between capacitor material and battery

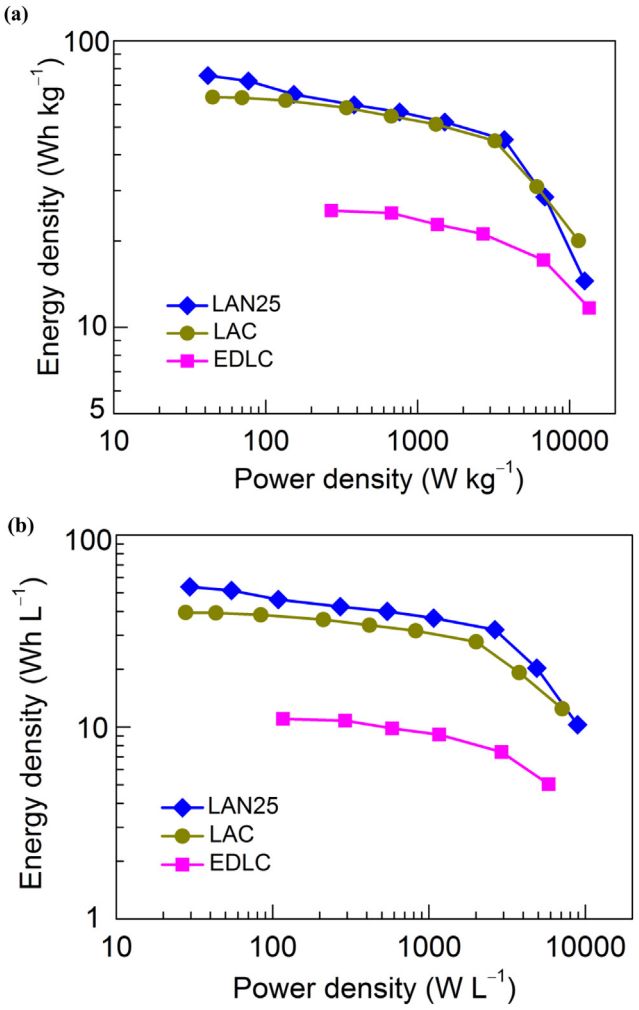

Fig. 7. Ragone plots for the LAC, LAN25 and EDLC capacitors on the (a) gravimetric and (b) volumetric basises.

material in the bifunctional cathode. In the present work, the optimal relative amount of NCM in composite cathode is 0.25. Compared with the internal serial hybridization system LAC, the volumetric energy densities of LAN25 increase 36% with little sacrifice of rate capability and cycleability. In this case, the relative capacitive contribution to the total capacity for cathode is estimated to be 47%. Another important factor to be considered is the potential swing ranges for both electrodes, which can be controlled by the cathode/anode electrode mass ratio and the pre-lithiation degree of HC. The upper potential of the bifunctional cathode is recommended to be lower than 4.2 V vs. Li^+/Li, and the lower potential of HC electrode should be higher than 0.1 V vs. Li^+/Li.

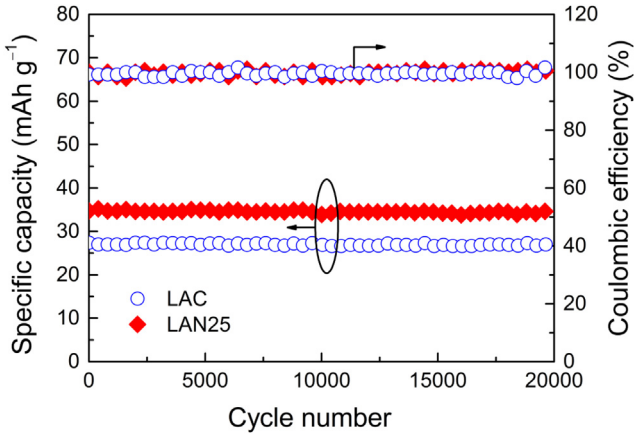

Fig. 8. Cyclic stability of the LAC ($m_+/m_- = 0.63$) and LAN25 ($m_+/m_- = 0.75$) lithium-ion hybrid capacitors during the voltage range of 2.5–3.9 V at a current density of 0.5 A g^{-1}.

4. Conclusion

In the present work, the rate capabilities of hard carbon, graphite and mesocarbon microbeads were comparatively studied, revealing that hard carbon materials have the highest rate capability. Moreover, the bifunctional electrodes (AC + NCM) were characterized by voltage profiles and *dQ*/*dV* curves using coin cells with Li plate as counter electrode, which confirm the internal parallel hybridization behavior of capacitor and battery components. Finally, the three-electrode lithium-ion hybrid capacitors with pre-lithiated hard carbon anode and (AC + NCM) bifunctional cathode electrodes were assembled employing a flexible package. The results show that the volumetric energy density of hybrid capacitor with bifunctional cathode can be improved by 36% with little sacrifice of rate capability and cycleability by the addition of 25 wt.% NCM in cathode electrode.

Acknowledgments

This work was supported by the National Natural Science Foundation of China (Nos. 51025726 and 51307167).

References

[1] P. Simon, Y. Gogotsi, Nat. Mater. 7 (2008) 845–854.
[2] D.J. Rand, J. Solid State Electrochem. 15 (2011) 1579–1622.
[3] A. Du Pasquier, I. Plitz, J. Gural, F. Badway, G.G. Amatucci, J. Power Sources 136 (2004) 160–170.
[4] H.S. Choi, C.R. Park, J. Power Sources 259 (2014) 1–14.
[5] D. Cericola, P. Novak, A. Wokaun, R. Kötz, J. Power Sources 196 (2011) 10305–10313.
[6] G.G. Amatucci, F. Badway, A. Du Pasquier, T. Zheng, J. Electrochem. Soc. 148 (2001) A930–A939.
[7] A. Du Pasquier, I. Plitz, S. Menocal, G. Amatucci, J. Power Sources 115 (2003) 171–178.
[8] M.M. Hantel, T. Kaspar, R. Nesper, A. Wokaun, R. Kötz, ECS Electrochem. Lett. 1 (2012) A1–A3.
[9] S.R. Sivakkumar, A.S. Milev, A.G. Pandolfo, Electrochim. Acta 56 (2011) 9700–9706.
[10] S.R. Sivakkumar, J.Y. Nerkar, A.G. Pandolfo, Electrochim. Acta 55 (2010) 3330–3335.
[11] M. Schroeder, M. Winter, S. Passerini, A. Balducci, J. Power Sources 238 (2013) 388–394.
[12] M. Schroeder, M. Winter, S. Passerini, A. Balducci, J. Electrochem. Soc. 159 (2012) A1240–A1245.
[13] J.H. Kim, J.S. Kim, Y.G. Lim, J.G. Lee, Y.J. Kim, J. Power Sources 196 (2011) 10490–10495.
[14] J.J. Ren, L.W. Su, X. Qin, M. Yang, J.P. Wei, Z. Zhou, P.W. Shen, J. Power Sources 264 (2014) 108–113.
[15] S.-K. Ahn, J.-J. Yang, H.-I. Kim, H. Habazaki, S.-G. Park, Chem. Lett. 43 (2014) 898–900.
[16] G. Gourdin, P.H. Smith, T. Jiang, T.N. Tran, D.Y. Qu, J. Electroanal. Chem. 688 (2013) 103–112.
[17] C. Decaux, G. Lota, E. Raymundo-Pinero, E. Frackowiak, F. Beguin, Electrochim. Acta 86 (2012) 282–286.
[18] W.J. Cao, J.P. Zheng, J. Power Sources 213 (2012) 180–185.
[19] W.J. Cao, J.P. Zheng, J. Electrochem. Soc. 160 (2013) A1572–A1576.
[20] W.J. Cao, J. Shih, J.P. Zheng, T. Doung, J. Power Sources 257 (2014) 388–393.
[21] S.R. Sivakkumar, A.G. Pandolfo, Electrochim. Acta 65 (2012) 280–287.
[22] J. Zhang, Z. Shi, C. Wang, Electrochim. Acta 125 (2014) 22–28.
[23] X.B. Hu, Y.J. Huai, Z.J. Lin, J.S. Suo, Z.H. Deng, J. Electrochem. Soc. 154 (2007) A1026–A1030.
[24] S.L. Chen, H.C. Hu, C.Q. Wang, G.L. Wang, J.L. Yin, D.X. Cao, J. Renew. Sustain. Energy 4 (2012) 033114.
[25] N. Böckenfeld, T. Placke, M. Winter, S. Passerini, A. Balducci, Electrochim. Acta 76 (2012) 130–136.

[26] X.B. Hu, Z.H. Deng, J.S. Suo, Z.L. Pan, J. Power Sources 187 (2009) 635–639.
[27] D. Cericola, P. Novak, A. Wokaun, R. Kötz, Electrochim. Acta 56 (2011) 1288–1293.
[28] D. Cericola, P. Novak, A. Wokaun, R. Kötz, Electrochim. Acta 56 (2011) 8403–8411.
[29] X.Z. Sun, X. Zhang, B. Huang, H.T. Zhang, D.C. Zhang, Y.W. Ma, J. Power Sources 243 (2013) 361–368.
[30] F. Wu, H.Q. Lu, Y.F. Su, S. Chen, Y.B. Guan, Mater. Sci. Forum 650 (2010) 142–149.
[31] M.S. Park, Y.G. Lim, J.H. Kim, Y.J. Kim, J. Cho, J.S. Kim, Adv. Energy Mater. 1 (2011) 1002–1006.
[32] M. Kim, F. Xu, J.-H. Lee, C. Jung, S.M. Hong, Q. Zhang, C.M. Koo, J. Mater. Chem. A 2 (2014) 10029–10033.
[33] A. Rudge, J. Davey, I. Raistrick, S. Gottesfeld, J.P. Ferraris, J. Power Sources 47 (1994) 89–107.
[34] J.R. Dahn, W. Xing, Y. Gao, Carbon 35 (1997) 825–830.
[35] F. Pico, J. Ibanez, T.A. Centeno, C. Pecharroman, R.M. Rojas, J.M. Amarilla, J.M. Rojo, Electrochim. Acta 51 (2006) 4693–4700.
[36] B. Wang, Q.M. Wang, B.H. Xu, T.F. Liu, D.L. Wang, G. Zhao, RSC Adv. 3 (2013) 20024–20033.
[37] X.Z. Sun, X. Zhang, H.T. Zhang, B. Huang, Y.W. Ma, J. Solid State Electrochem 17 (2013) 2035–2042.
[38] H.H. Zheng, J. Li, X.Y. Song, G. Liu, V.S. Battaglia, Electrochim. Acta 71 (2012) 258–265.